Application of the CE/SE method to two-dimensional flow in fluid film bearings

Sorin Cioc and Theo G. Keith, Jr
Mechanical Engineering Department, The University of Toledo, Toledo, Ohio, USA

Received February 2002
Revised October 2002
Accepted October 2002

Keywords *Bearings, Fluid, Flow, Numerical analysis*

Abstract *A numerical scheme that has been successfully used to solve a wide variety of compressible flow problems, entitled the space-time conservation element and solution element (CE/SE) method, is extended to predict the effects of gaseous cavitation in moderate to heavily loaded bearings. The formulation of the two-dimensional, finite length, bearing problem is presented. The numerical results obtained are compared with other numerical solutions to demonstrate the superior ability of the method to solve such problems.*

Nomenclature

a = $\frac{U}{2} + g_c \frac{\beta' h}{12\mu} \frac{\partial h}{\partial x}$ for the dimensional form of the governing equation
= $\frac{1}{4\pi} + g_c \frac{\bar{\beta}\bar{h}}{48\pi^2} \frac{\partial \bar{h}}{\partial \bar{x}}$ for the non-dimensional form of the governing equation

b = $g_c \frac{\beta' h^2}{12\mu}$ for the dimensional form of the governing equation
= $g_c \frac{\bar{\beta}\bar{h}^2}{48\pi^2}$ for the non-dimensional form of the governing equation

c = $g_c \frac{\beta' h^2}{12\mu} \frac{\partial h}{\partial z}$ for the dimensional form of the governing equation
= $g_c \frac{\bar{\beta}\bar{h}}{48\pi^2} \frac{\partial \bar{h}}{\partial \bar{z}}$ for the non-dimensional form of the governing equation

C = radial clearance

d = $g_c \frac{\beta' h^2}{12\mu}$ for the dimensional form of the governing equation
= $g_c \frac{\bar{\beta}\bar{h}^2}{48\pi^2}$ for the non-dimensional form of the governing equation

f = $au - b\frac{\partial u}{\partial x}$ flux term in x direction

$\vec{F}$ = $f\vec{i} + g\vec{k}$ vector flux term

g = $cu - d\frac{\partial u}{\partial z}$ flux term in z direction

g_c = switch function

h = film thickness

$\bar{h}$ = h/C non-dimensional film thickness

$\vec{i}, \vec{k}$ = unit vectors in circumferential and in axial directions, respectively

L = length of the bearing (in axial direction)

$\vec{n}$ = unit vector normal on the contour line, oriented outwards

p = fluid pressure

p_c = cavitation pressure

t = time

u = $h\theta$ for the dimensional form of the governing equation
= $\bar{h}\theta$ for the non-dimensional form of the governing equation

U = velocity in circumferential direction (ωR)

x = circumferential coordinate

$\bar{x}$ = $x/(2\pi R)$ non-dimensional circumferential coordinate

International Journal of Numerical Methods for Heat & Fluid Flow
Vol. 13 No. 2, 2003
pp. 216-243

0961-5539
DOI 10.1108/09615530310459351

z = axial coordinate
$\bar{z}$ = $z/(2\pi R)$ non-dimensional axial coordinate
α = exponent used in the second form of artificial dissipation
β = weight parameter characterizing the second form of artificial dissipation
β' = bulk modulus
$\bar{\beta}'$ = $\frac{\beta'}{\mu\omega}\left(\frac{C}{R}\right)^2$ non-dimensional bulk modulus
Δt = time step
ε = weight parameter characterizing the first form of artificial dissipation
μ = fluid viscosity
ρ = fluid density
ρ_c = fluid density at cavitation pressure
θ = ρ/ρ_c non-dimensional density in full film
= fractional film content in cavitated region
ω = angular velocity of the journal bearing

Subscripts and superscripts

$(\,)_0$ = value of the variable in the point O
$(\,)_x$, $(\,)_z$, $(\,)_t$ = partial derivative with respect to x, z, and t, respectively
$(\,)^a$ = value obtained in the scheme without artificial dissipation
$(\,)^c$ = derivative calculated using a central difference formula
$(\,)^{a-\varepsilon}$ = derivative calculated using the $a-\varepsilon$ scheme
$(\,)^{a-\varepsilon-\alpha-\beta}$ = derivative calculated using the $a-\varepsilon-\alpha-\beta$ scheme
$(\,)^n$ = time step n
$(\,)^w$ = derivative calculated using non-linear weighted averaging

Introduction

The space-time conservation element and solution element (CE/SE) method was proposed for the first time by Chang and To (1991). Over the past several years it has been utilized in a number of fluid flow applications that involve shock waves, contact discontinuities, acoustic waves, vortices and chemical reactions. One of its main features is that it can simultaneously capture small and large discontinuities (such as sound waves and shock waves) without introducing numerical oscillations in the solution (Chang *et al.*, 1999; Qin *et al.*, 2001; Wang *et al.*, 2000). Accordingly, this new method is an excellent candidate to be applied to the flow in cavitated bearings.

Historically, the effect of cavitation on the performance of bearings was disregarded in numerical calculations. The common practice, known as Gümbel (or half-Sommerfeld) boundary conditions, was to modify full film results by setting negative relative pressures to zero (relative to the cavitation pressure). Although the load carrying predictions were reasonably accurate, the results violated the mass conservation principle. Consequently, several other procedures have been proposed. Jakobsson and Floberg (1957) and later Olsson (1965) introduced a set of self-consistent boundary conditions for cavitation to be applied to Reynolds equation. This procedure is valid for moderate to heavy loaded bearings and is generally called JFO theory. This methodology is commonly incorporated into modern computational algorithms for bearings, and is also implicitly included in the present method.

Previous computational methods used for this problem are known to have some difficulties. Elrod's algorithm (Elrod, 1981) necessitated, as the author

pointed out, "considerable experimentation" to develop the algorithm. It has only first order accuracy in the cavitated region, while in the full film region, the algorithm is second order accurate; an oscillation in the cavitation front is often found to occur. The method proposed by Vijayaraghavan and Keith (1989) is based on concepts that were used in transonic flow (Vijayaraghavan *et al.*, 1990). Their method uses a number of features from the Elrod algorithm, but does not "rely on experimentation" to develop the solver. It should be noted that the method proposed by Vijayaraghavan and Keith has the same accuracy as the Elrod's algorithm in cavitated regions and in the full film region and, like Elrod's method, loses accuracy at the cavitation boundaries.

In this context, a method that is conceptually simple and has the capacity to accurately predict the fluid film flow including the boundaries of the cavitated region(s), without numerical oscillations or smearing, is welcomed.

The CE/SE method applied to the Reynolds equation has some noticeable advantages: it is second order over the entire domain, it computes in an unified way the pressure induced flow for all the regions and, because it solves a set of integral equations derived directly from the physical conservation laws, the scheme is able to naturally capture the flow discontinuities (cavitation boundaries). As also shown by the one-dimensional application (Cioc and Keith, 2002), the CE/SE method can provide better results for the cavitation and reformation front positions, as well as for the distributions of the state variables in their vicinity.

Analysis

Analytical formulation

The two-dimensional, transient Reynolds equation, written for a Newtonian compressible fluid in laminar flow, is

$$\frac{\partial \rho h}{\partial t} + \frac{\partial}{\partial x}\left(\frac{\rho h U}{2} - \frac{\rho h^3}{12\mu}\frac{\partial p}{\partial x}\right) + \frac{\partial}{\partial z}\left(-\frac{\rho h^3}{12\mu}\frac{\partial p}{\partial z}\right) = 0. \tag{1}$$

The density of the lubricant is related to the film pressure through the definition of the bulk modulus β'

$$\beta' = \rho\frac{\partial p}{\partial \rho}. \tag{2}$$

In order to work in terms of density, a non-dimensional density variable, θ is introduced

$$\theta = \frac{\rho}{\rho_c}, \tag{3}$$

where ρ_c is the density of the lubricant at the cavitation pressure, considered constant. In this case the bulk modulus definition becomes

$$\beta' = \theta \frac{\partial p}{\partial \theta}. \tag{4}$$

The Reynolds equation yields, in terms of the non-dimensional density

$$\frac{\partial \rho_c h\theta}{\partial t} + \frac{\partial}{\partial x}\left(\frac{\rho_c h\theta U}{2} - \frac{\rho_c \beta' h^3}{12\mu}\frac{\partial \theta}{\partial x}\right) + \frac{\partial}{\partial z}\left(-\frac{\rho_c \beta' h^3}{12\mu}\frac{\partial \theta}{\partial z}\right) = 0. \tag{5}$$

Considering that in the cavitation region the flow induced by the pressure is negligible, i.e.

$$\begin{aligned} \frac{\partial}{\partial x}\left(\frac{\rho h^3}{12\mu}\frac{\partial p}{\partial x}\right) = \frac{\partial}{\partial x}\left(\frac{\rho_c \beta' h^3}{12\mu}\frac{\partial \theta}{\partial x}\right) \cong 0, \\ \frac{\partial}{\partial z}\left(\frac{\rho h^3}{12\mu}\frac{\partial p}{\partial z}\right) = \frac{\partial}{\partial z}\left(\frac{\rho_c \beta' h^3}{12\mu}\frac{\partial \theta}{\partial z}\right) \cong 0, \end{aligned} \tag{6}$$

a switch function, g_c,

$$g_c = \begin{cases} 1 \text{-} \textit{full film region} \\ 0 \text{-} \textit{cavitated region} \end{cases} \tag{7}$$

is introduced into the pressure-density relation

$$g_c \beta' = \rho \frac{\partial p}{\partial \rho}, \tag{8}$$

so that the Reynolds equation can be written as

$$\frac{\partial \rho_c h\theta}{\partial t} + \frac{\partial}{\partial x}\left(\frac{\rho_c h\theta U}{2} - g_c \frac{\rho_c \beta' h^3}{12\mu}\frac{\partial \theta}{\partial x}\right) - \frac{\partial}{\partial z}\left(g_c \frac{\rho_c \beta' h^3}{12\mu}\frac{\partial \theta}{\partial z}\right) = 0. \tag{9}$$

The pressure-density relation yields, by direct integration,

$$p = p_c + g_c \beta' \ln \theta, \tag{10}$$

where the cavitation pressure p_c is a constant as a result of the switch function assumption.

Numerical formulation

A more suitable form of equation (9) for the numerical formulation can be obtained using a new variable u

$$u = h\theta. \tag{11}$$

In terms of u, the Reynolds equation can be written as

$$\frac{\partial u}{\partial t}+\frac{\partial f}{\partial x}+\frac{\partial g}{\partial z}=0, \tag{12}$$

where the flux terms f and g are,

$$f=au-b\frac{\partial u}{\partial x}, \quad g=cu-d\frac{\partial u}{\partial z}, \tag{13}$$

and the coefficients a, b, c and d are

$$a=\frac{U}{2}+g_c\frac{\beta' h}{12\mu}\frac{\partial h}{\partial x}, \quad b=d=g_c\frac{\beta' h^2}{12\mu}, \quad c=g_c\frac{\beta' h}{12\mu}\frac{\partial h}{\partial z}. \tag{14}$$

In non-dimensional form, equation (12) has the same expression, with

$$a=\frac{1}{4\pi}+g\frac{\bar{\beta}'\bar{h}}{48\pi^2}\frac{\partial \bar{h}}{\partial \bar{x}}, \quad b=d=g\frac{\bar{\beta}'\bar{h}^2}{48\pi^2}, \quad c=g\frac{\bar{\beta}'\bar{h}}{48\pi^2}\frac{\partial \bar{h}}{\partial \bar{z}}, \quad u=\bar{h}\theta.$$

All coefficients a, b, c and d are functions of space x and z. If the geometry is time dependent, then the film is expressed as $h=h(x,z,t)$, and these coefficients are also time dependent. However, when developing the numerical algorithm, these coefficients are considered to be locally constant.

A first order Taylor series for the unknown function u, starting from an expansion point $O(x_0,z_0,t_0)$ is

$$u\cong u_0+(u_x)_0(x-x_0)+(u_z)_0(z-z_0)+(u_t)_0(t-t_0), \tag{15}$$

where the time derivative, in conformity with equation (12), can be written as

$$(u_t)_0=-\left(\frac{\partial f}{\partial x}\right)_0-\left(\frac{\partial g}{\partial z}\right)_0. \tag{16}$$

Since the flux terms f and g can be considered as functions of the unknown u and its space derivatives $f=f(u,u_x,u_z)$, $g=g(u,u_x,u_z)$ using a first order approximation, we may write that

$$\frac{\partial f}{\partial x}\cong\frac{\partial f}{\partial u}u_x=au_x, \quad \frac{\partial g}{\partial z}\cong\frac{\partial g}{\partial u}u_z=cu_z. \tag{17}$$

Accordingly, equation (15) becomes

$$u\cong u_0+(u_x)_0(x-x_0)+(u_z)_0(z-z_0)-[a_0(u_x)_0+c_0(u_z)_0](t-t_0). \tag{18}$$

In the same way functions f and g are approximated as

$$f \cong \left(\frac{\partial f}{\partial u}\right)_0 u + \left(\frac{\partial f}{\partial u_x}\right)_0 u_x + \left(\frac{\partial f}{\partial u_z}\right)_0 u_z = a_0 u - b_0 u_x,$$
$$g \cong \left(\frac{\partial g}{\partial u}\right)_0 u + \left(\frac{\partial g}{\partial u_x}\right)_0 u_x + \left(\frac{\partial g}{\partial u_z}\right)_0 u_z = c_0 u - d_0 u_z. \tag{19}$$

Alternately, considering that in the vicinity of the expansion point $O(x_0, z_0, t_0)$, $u_x \cong \text{const.} = (u_x)_0$, $u_z \cong \text{const.} = (u_z)_0$ and substituting the expression of u from equation (18) into equation (19) yields

$$f \cong a_0 u_0 - b_0 (u_x)_0 + a_0 (u_x)_0 (x - x_0) + a_0 (u_z)_0 (z - z_0) - \left[a_0^2 (u_x)_0 + a_0 c_0 (u_z)_0\right](t - t_0),$$
$$g \cong c_0 u_0 - d_0 (u_z)_0 + c_0 (u_x)_0 (x - x_0) + c_0 (u_z)_0 (z - z_0) - \left[a_0 c_0 (u_x)_0 + c_0^2 (u_z)_0\right](t - t_0). \tag{20}$$

Consider a triangular mesh in the (x, z) plane. One triangle BCD and its three neighbor elements are shown in Figure 1. Point A is the centroid of the triangle BCD, while points E, F and G are the centroids of the neighbor triangles BCH, CDI and BDJ.

The CE/SE method calculates the values of the dependent variables u, u_x, u_z for point A at the time step $t = t^{n+\frac{1}{2}}$ using the corresponding values of the same variables for the points E, F and G at the time step $t = t^n$. In order to calculate the three unknowns at the new time step, a system of three equations will be

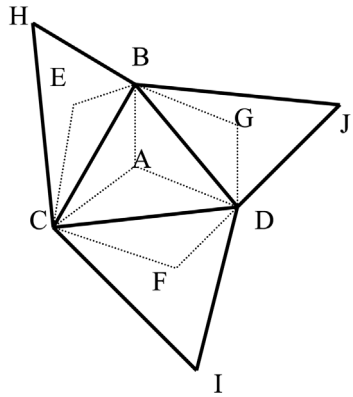

Figure 1.
Triangular mesh element and its neighbors

derived. One equation can be obtained considering the quadrilateral *ABEC*. Integrating simultaneously the governing equation (equation (12)), over the surface of this quadrilateral and in time, between time steps t^n and $t^{n+\frac{1}{2}}$ (see Figure 2), yields

$$\iint_{ABEC}\int_{t^n}^{t^{n+\frac{1}{2}}}\frac{\partial u}{\partial t}\,\mathrm{d}t\,\mathrm{d}\sigma+\int_{t^n}^{t^{n+\frac{1}{2}}}\iint_{ABEC}\left[\frac{\partial}{\partial x}(au-bu_x)+\frac{\partial}{\partial z}(cu-du_z)\right]\mathrm{d}\sigma\mathrm{d}t=0. \tag{21}$$

Equation (21) implies flux conservation in the three-dimensional space (x, z, t). Performing the time integration for the first term and transforming the surface integration into a contour integration for the second term (using Green theorem) yields

$$\iint_{ABEC}\left(u^{n+\frac{1}{2}}-u^n\right)\mathrm{d}\sigma+\int_{t^n}^{t^{n+\frac{1}{2}}}\oint_{ABEC}\vec{F}\cdot\vec{n}\,\mathrm{d}s\,\mathrm{d}t=0, \tag{22}$$

where $\vec{n}$ is the outward directed unit vector normal to the contour, and

$$\vec{F}=f\vec{i}+g\vec{k} \tag{23}$$

is a vector in the (x, z) plane characterized by the Cartesian unit vectors $(\vec{i},\vec{k})$. Functions f and g are given by equation (13).

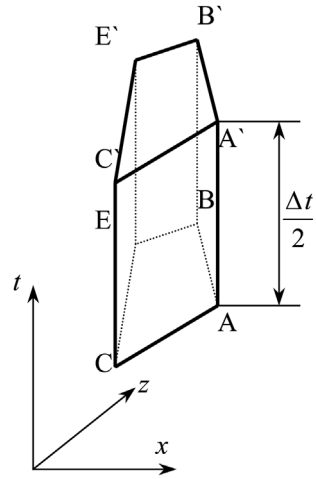

Figure 2.
Conservation volume in the (x, z, t) space

Functions u, f, g are next substituted with linear approximations (see equations (18) and (20)), so that equation (22) can be written as

$$\left(u_{ABEC}^{n+\frac{1}{2}} - u_{ABEC}^{n}\right)A_{ABEC} + \frac{\Delta t}{2}\left(\oint_{ABEC} \vec{F}\cdot\vec{n}\,\mathrm{d}s\right)^{n+\frac{1}{4}} = 0, \tag{24}$$

where $u_{ABEC}^{n+\frac{1}{2}}$ and u_{ABEC}^{n} designate the value of u in the center of the quadrilateral $ABEC$ at the time steps $n+\frac{1}{2}$ and n, A_{ABEC} is the area of the quadrilateral $ABEC$ and the contour integration is calculated at the time $t^{n+\frac{1}{4}} = t^{n} + \frac{\Delta t}{4}$. The values $u_{ABEC}^{n+\frac{1}{2}}$ and u_{ABEC}^{n} are evaluated from equation (18) using the Taylor expansion point $A'(x_{A'}, z_{A'})$ at the time step $t^{n+\frac{1}{2}}$ and $E'(x_{E'}, z_{E'})$ at the time step t^{n}, respectively. This yields,

$$\begin{aligned} u_{ABEC}^{n+\frac{1}{2}} &= u_{A'}^{n+\frac{1}{2}} + (x_{ABEC} - x_{A'})\frac{\partial u}{\partial x}\bigg|_{A'}^{n+\frac{1}{2}} + (z_{ABEC} - z_{A'})\frac{\partial u}{\partial z}\bigg|_{A'}^{n+\frac{1}{2}}, \\ u_{ABEC}^{n} &= u_{E'}^{n} + (x_{ABEC} - x_{E'})\frac{\partial u}{\partial x}\bigg|_{E'}^{n} + (z_{ABEC} - z_{E'})\frac{\partial u}{\partial z}\bigg|_{E'}^{n}. \end{aligned} \tag{25}$$

Note that the expansion points are not necessarily the centers of the triangular elements, but can be chosen in any suitable way.

The contour integral from the second term in equation (24) can be divided into four line integrals along the sides of the quadrilateral.

$$\begin{aligned} \oint_{ABEC} \vec{F}^{n+\frac{1}{4}}\cdot\vec{n}\,\mathrm{d}s = &\int_{AB} \vec{F}^{n+\frac{1}{4}}\cdot\vec{n}_{AB}\,\mathrm{d}s + \int_{BE} \vec{F}^{n+\frac{1}{4}}\cdot\vec{n}_{BE}\,\mathrm{d}s \\ &+ \int_{EC} \vec{F}^{n+\frac{1}{4}}\cdot\vec{n}_{EC}\,\mathrm{d}s + \int_{CA} \vec{F}^{n+\frac{1}{4}}\cdot\vec{n}_{CA}\,\mathrm{d}s. \end{aligned} \tag{26}$$

Each of these four line integrals, consistent with the previous approximations, is calculated considering that each integrand has a linear form. From the mean value theorem of calculus, the value of each line integral is equal to the value of the integrand at the mid-point of the line segment multiplied by the length of the segment. For the segment AB, considering $\left(A', t^{n+\frac{1}{2}}\right)$ as the Taylor series expansion point in equation (20), yields

$$\int_{AB} \vec{F}^{n+\frac{1}{4}} \cdot \vec{\mathrm{n}}_{AB} = [f n_{xAB} + g n_{zAB}]_{\frac{A+B}{2}}^{n+\frac{1}{4}} L_{AB}$$

$$= \left[(au - bu_x)\big|_{A'}^{n+\frac{1}{2}} + (au_x)\big|_{A'}^{n+\frac{1}{2}} \left(\frac{x_A + x_B}{2} - x_{A'} \right) + (au_z)\big|_{A'}^{n+\frac{1}{2}} \left(\frac{z_A + z_B}{2} - z_{A'} \right) \right.$$

$$\left. + (a^2 u_x + acu_z)_{A'}^{n+\frac{1}{2}} \frac{\Delta t}{4} \right] (z_B - z_A) \tag{27}$$

$$- \left[(cu - du_z)\big|_{A'}^{n+\frac{1}{2}} + (cu_x)\big|_{A'}^{n+\frac{1}{2}} \left(\frac{x_A + x_B}{2} - x_{A'} \right) + (cu_z)\big|_{A'}^{n+\frac{1}{2}} \left(\frac{z_A + z_B}{2} - z_{A'} \right) \right.$$

$$\left. + \left(acu_x + c^2 u_z \right)_{A'}^{n+\frac{1}{2}} \frac{\Delta t}{4} \right] (x_B - x_A)$$

In equation (27), the exterior unit normal to the segment AB of length L_{AB} has been substituted with its expression,

$$\vec{n}_{AB} = n_{xAB}\vec{i} + n_{zAB}\vec{j} = \frac{(z_B - z_A)\vec{i} - (x_B - x_A)\vec{j}}{L_{AB}}. \tag{28}$$

Similar expressions can be written for the other three line integrals of equation (26). Note that the Taylor expansions must be performed starting from point $\left(A', t^{n+\frac{1}{2}}\right)$ for the line integrals

$$\int_{AB} \vec{F}^{n+\frac{1}{4}} \cdot \vec{n}_{AB} \, \mathrm{d}s$$

and

$$\int_{CA} \vec{F}^{n+\frac{1}{4}} \cdot \vec{n}_{CA} \, \mathrm{d}s,$$

while for the integrals

$$\int_{BE} \vec{F}^{n+\frac{1}{4}} \cdot \vec{n}_{BE} \, \mathrm{d}s$$

and

$$\int_{EC} \vec{F}^{n+\frac{1}{4}} \cdot \vec{n}_{EC} \, \mathrm{d}s$$

point (E', t^n) must be considered. Since the calculations can be relatively complicated for a generic grid, a symbolic mathematical code (MAPLE) was

used. Performing all the calculations and substituting into equation (22) yields the first equation for the considered triangular element

$$a_1 u_{A'}^{n+\frac{1}{2}} + b_1 (u_x)_{A'}^{n+\frac{1}{2}} + c_1 (u_z)_{A'}^{n+\frac{1}{2}} + d_1 u_{E'}^{n} + e_1 (u_x)_{E'}^{n} + f_1 (u_z)_{E'}^{n} = 0, \qquad (29a)$$

where a_1, b_1, c_1, d_1, e_1, f_1 are coefficients that depend on the geometry (coordinates of points A, A', E, E', B, C and the center of quadrilateral $ABEC$) and on the governing equation coefficients a, b, c, d given by equation (14), evaluated at points A' and E' at the time steps $n + \frac{1}{2}$ and n, respectively.

Considering the quadrilaterals $ACFD$ and $ADGB$, two additional equations similar to equation (29(a)) are developed

$$a_2 u_{A'}^{n+\frac{1}{2}} + b_2 (u_x)_{A'}^{n+\frac{1}{2}} + c_2 (u_z)_{A'}^{n+\frac{1}{2}} + d_2 u_{F'}^{n} + e_2 (u_x)_{F'}^{n} + f_2 (u_z)_{F'}^{n} = 0, \qquad (29b)$$

$$a_3 u_{A'}^{n+\frac{1}{2}} + b_3 (u_x)_{A'}^{n+\frac{1}{2}} + c_3 (u_z)_{A'}^{n+\frac{1}{2}} + d_3 u_{G'}^{n} + e_3 (u_x)_{G'}^{n} + f_3 (u_z)_{G'}^{n} = 0. \qquad (29c)$$

All values at the time step n (previous half-time step) are known, so that equations (29(a)-(c)) form a system of three equations with three unknowns $u_{A'}^{n+\frac{1}{2}}, (u_x)_{A'}^{n+\frac{1}{2}}, (u_z)_{A'}^{n+\frac{1}{2}}$. Written in this form, the method is locally implicit. Note that the coefficients of the system, being functions of the coefficients a, b, c, d given by equation (14), depend also on the unknown $u_{A'}^{n+\frac{1}{2}}$ through the switch coefficient g_c. An iterative method to solve this system is appropriate.

An alternate approach is to choose the Taylor series expansion point A' as the center of the hexagon $BECFDG$. The other three Taylor series expansion points E', F', G' can be chosen arbitrarily; however, in order to maintain consistency, they are chosen as the centers of the corresponding hexagons formed around the neighboring triangular elements. Note that the values of the dependent variables at time step n, i.e. u, u_x, u_z, must be known at these points. Note also that, as with the previous approximations, the values of the derivatives u_x, u_z at any given time step are considered constant on the surface of a triangular element (such as BCD), while the value of the variable u at the same time step can be calculated using the first order Taylor expansion (equation (15)).

Adding equations (29(a)-(c)) yields a new equation that represents the flux conservation over the hexagon and over one half-time step. When point A' is the center of the hexagon $BECFDG$, this equation has a simpler form given by

$$\begin{aligned} a_{\text{sum}} u_{A'}^{n+\frac{1}{2}} &+ d_1 u_{E'}^{n} + e_1 (u_x)_{E'}^{n} + f_1 (u_z)_{E'}^{n} + d_2 u_{F'}^{n} + e_2 (u_x)_{F'}^{n} + f_2 (u_z)_{F'}^{n} \\ &+ d_3 u_{G'}^{n} + e_3 (u_x)_{G'}^{n} + f_3 (u_z)_{G'}^{n} = 0, \end{aligned} \qquad (30)$$

where

$$a_{\text{sum}} = A_{ABEC} + A_{ACFD} + A_{ADGB} = A_{BECFDG}. \tag{31}$$

This equation has only one unknown, $u_{A'}^{n+\frac{1}{2}}$, and can easily be solved explicitly. It is also important to note that all the coefficients in equation (30) depend only on the geometry (coordinates of the points) and the values of the dependent variables at the previous half-time step so that no iterative method is needed.

After calculating the value $u_{A'}^{n+\frac{1}{2}}$, the values of the other two dependent variables $(u_x)_{A'}^{n+\frac{1}{2}}$ and $(u_z)_{A'}^{n+\frac{1}{2}}$ can be calculated using any two of the equations in the set, equations (29(a)-(c)). Since $u_{A'}^{n+\frac{1}{2}}$ is known at this stage of calculations, the value of g_c is also known, so that all coefficients in equations (29(a)-(c)) are determined.

In the original form, also known as the a form, the algorithm is "non-dissipative if it is stable" (Chang *et al.*, 1998). In order to insure stability (not only neutral stability), the method must have at least some form of artificial dissipation. The authors of the method have proposed two forms: the $a - \varepsilon$ scheme and the $a - \varepsilon - \alpha - \beta$ scheme. Both schemes differ from the a scheme only in the way the derivatives $(u_x)_{A'}^{n+\frac{1}{2}}$ and $(u_z)_{A'}^{n+\frac{1}{2}}$ are calculated. Since the value $u_{A'}^{n+\frac{1}{2}}$ is computed from equation (30), the flux conservation over the boundary of the hexagon *BECFDG* and in time is still insured. However, because the derivatives $(u_x)_{A'}^{n+\frac{1}{2}}$ and $(u_z)_{A'}^{n+\frac{1}{2}}$ are not calculated from the system, equations (29(a)-(c)), the flux conservation is not insured in this case over each of the quadrilaterals *ABEC*, *ACFD* and *ADGB*.

The $a-\varepsilon$ scheme starts from the principle that central differencing computation of the derivatives provides numerical dissipation. In this scheme, the values of the dependent variable u at the new time step $n+\frac{1}{2}$ are evaluated at three new points E'', F'', G''. Let A'' be the center of the triangle $E'F'G'$ (Figure 3) and let $\overrightarrow{A''A'}$ be the vector that displaces points E', F', G' into the three new points E'', F'', G'' respectively, i.e.

$$\overrightarrow{A''A'} = \overrightarrow{E'E''} = \overrightarrow{F'F''} = \overrightarrow{G'G''} \tag{32}$$

This procedure insures that the center of the triangle $E''F''G''$ coincides with point A'.

The values $u_{E''}^{n+\frac{1}{2}}, u_{F''}^{n+\frac{1}{2}}$ and $u_{G''}^{n+\frac{1}{2}}$ can easily be computed using Taylor expansion (equation (18)) with the expansion points E', F', G', respectively, and at the time step n. For instance,

$$\begin{aligned} u_{E''}^{n+\frac{1}{2}} = u_{E'}^{n} + \left(x_{E''} - x_{E'}\right)\left(u_x\right)_{E'}^{n} + \left(z_{E''} - z_{E'}\right)\left(u_z\right)_{E'}^{n} \\ - \frac{\Delta t}{2}\left[a_{E'}^{n}\left(u_x\right)_{E'}^{n} + c_{E'}^{n}\left(u_z\right)_{E'}^{n}\right]. \end{aligned} \tag{33}$$

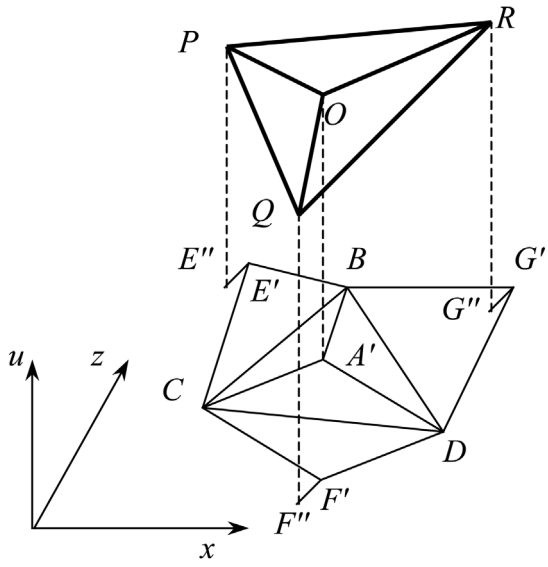

Figure 3.
The (x, z, u) space considered for $a - \varepsilon$ and $a - \varepsilon - \alpha - \beta$ schemes

Similar expressions are used for the calculation of $u_{F''}^{n+\frac{1}{2}}$ and $u_{G''}^{n+\frac{1}{2}}$. Consider also the value $u_{A'}^{n+\frac{1}{2}}$ calculated from equation (30). In the space (x, z, u), four points can be defined: $O\left(x_{A'}, z_{A'}, u_{A'}^{n+\frac{1}{2}}\right)$, $P\left(x_{E''}, z_{E''}, u_{E''}^{n+\frac{1}{2}}\right)$, $Q\left(x_{F''}, z_{F''}, u_{F''}^{n+\frac{1}{2}}\right)$ and $R\left(x_{G''}, z_{G''}, u_{G''}^{n+\frac{1}{2}}\right)$, as shown in Figure 3. Consider four planes each defined by a set of three points: *OPQ*, *OQR*, *ORP* and *PQR*. In each of these planes function u is linear in both x and z, so that the values of its partial space, derivatives can easily be calculated.

In order to exemplify this simple procedure, consider the plane *OPQ*. In this plane, function u has the expression

$$u(x,z)_{OPQ} = \left(\frac{\partial u}{\partial x}\right)_{OPQ} x + \left(\frac{\partial u}{\partial z}\right)_{OPQ} z + u_0 \tag{34}$$

where u_0 is a constant, while $\left(\frac{\partial u}{\partial x}\right)_{OPQ}$ and $\left(\frac{\partial u}{\partial z}\right)_{OPQ}$ are the spatial partial derivatives corresponding to the triangle *OPQ*, derivatives that are to be determined. Imposing the conditions

$$\begin{aligned} &u(x_{A'}, z_{A'}) = u_{A'}^{n+\frac{1}{2}} \ (\text{point } O), \quad u(x_{E''}, z_{E''}) = u_{E''}^{n+\frac{1}{2}} \ (\text{point } P), \\ &u(x_{F''}, z_{F''}) = u_{F''}^{n+\frac{1}{2}} \ (\text{point } Q), \end{aligned} \tag{35}$$

and solving the linear system of three equations with three unknowns with Cramer's rule, the values of the spatial partial derivatives are

$$\left(\frac{\partial u}{\partial x}\right)_{OPQ} = \frac{\Delta_1}{\Delta}, \quad \left(\frac{\partial u}{\partial z}\right)_{OPQ} = \frac{\Delta_2}{\Delta}, \tag{36}$$

where Δ, Δ_1 and Δ_2 are the determinants

$$\Delta = \begin{vmatrix} x_{A'} & z_{A'} & 1 \\ x_{E''} & z_{E''} & 1 \\ x_{F''} & z_{F''} & 1 \end{vmatrix}, \quad \Delta_1 = \begin{vmatrix} u_{A'}^{n+\frac{1}{2}} & z_{A'} & 1 \\ u_{E''}^{n+\frac{1}{2}} & z_{E''} & 1 \\ u_{F''}^{n+\frac{1}{2}} & z_{F''} & 1 \end{vmatrix}, \quad \Delta_2 = \begin{vmatrix} x_{A'} & u_{A'}^{n+\frac{1}{2}} & 1 \\ x_{E''} & u_{E''}^{n+\frac{1}{2}} & 1 \\ x_{F''} & u_{F''}^{n+\frac{1}{2}} & 1 \end{vmatrix}. \tag{37}$$

Similar expressions can easily be deduced for the partial derivatives expressed in the other three planes *OQR*, *ORP* and *PQR*. Finally, define the "central" derivatives at point A' as the average values of the derivatives obtained for the three triangles *OPQ*, *OQR* and *ORP*, i.e.

$$\begin{aligned} (u_x^c)_{A'}^{n+\frac{1}{2}} &= \frac{1}{3}\left[\left(\frac{\partial u}{\partial x}\right)_{OPQ} + \left(\frac{\partial u}{\partial x}\right)_{OQR} + \left(\frac{\partial u}{\partial x}\right)_{ORP}\right], \\ (u_z^c)_{A'}^{n+\frac{1}{2}} &= \frac{1}{3}\left[\left(\frac{\partial u}{\partial z}\right)_{OPQ} + \left(\frac{\partial u}{\partial z}\right)_{OQR} + \left(\frac{\partial u}{\partial z}\right)_{ORP}\right]. \end{aligned} \tag{38}$$

Because, as shown earlier, point A' is the center of the triangle $E''F''G''$, the values obtained with equation (38) are the same as the values obtained for the plane *PQR*. Thus, $(u_x^c)_{A'}^{n+\frac{1}{2}}$ and $(u_z^c)_{A'}^{n+\frac{1}{2}}$ can be interpreted as central-difference estimates of the space derivatives at point A'. Note also that the computation of these derivatives is entirely explicit.

The $a - \varepsilon$ scheme considers a weighted average between the values of the derivatives calculated with the a scheme and the values obtained with equation (38)

$$\begin{aligned} \left(u_x^{a-\varepsilon}\right)_{A'}^{n+\frac{1}{2}} &= \left(u_x^a\right)_{A'}^{n+\frac{1}{2}} + 2\varepsilon\left[\left(u_x^c\right)_{A'}^{n+\frac{1}{2}} - \left(u_x^a\right)_{A'}^{n+\frac{1}{2}}\right], \\ \left(u_z^{a-\varepsilon}\right)_{A'}^{n+\frac{1}{2}} &= \left(u_z^a\right)_{A'}^{n+\frac{1}{2}} + 2\varepsilon\left[\left(u_z^c\right)_{A'}^{n+\frac{1}{2}} - \left(u_z^a\right)_{A'}^{n+\frac{1}{2}}\right]. \end{aligned} \tag{39}$$

Note that for $\varepsilon = 0.5$,

$$\left(u_x^{a-\varepsilon}\right)_{A'}^{n+\frac{1}{2}} = \left(u_x^c\right)_{A'}^{n+\frac{1}{2}}, \quad \left(u_z^{a-\varepsilon}\right)_{A'}^{n+\frac{1}{2}} = \left(u_z^c\right)_{A'}^{n+\frac{1}{2}},$$

so that the $a - \varepsilon$ scheme becomes completely explicit.

The $a-\varepsilon-\alpha-\beta$ scheme considers first the absolute values of the gradients of function u calculated in the three planes OPQ, OQR and ORP, i.e.

$$\theta_{OPQ}=\sqrt{(u_x)^2_{OPQ}+(u_z)^2_{OPQ}} \tag{40}$$

where $(u_x)_{OPQ}$ and $(u_z)_{OPQ}$ are calculated with equation (36). Similarly,

$$\theta_{OQR}=\sqrt{(u_x)^2_{OQR}+(u_z)^2_{OQR}},\quad \theta_{ORP}=\sqrt{(u_x)^2_{ORP}+(u_z)^2_{ORP}}. \tag{41}$$

Two new nonlinear weighted average values for the space derivatives can be computed

$$\begin{aligned}\left(u_x^w\right)_{A'}^{n+\frac{1}{2}}&=\frac{\left(\theta_{OQR}\theta_{ORP}\right)^{\alpha}\left(u_x\right)_{OPQ}+\left(\theta_{ORP}\theta_{OPQ}\right)^{\alpha}\left(u_x\right)_{OQR}+\left(\theta_{OPQ}\theta_{OQR}\right)^{\alpha}\left(u_x\right)_{ORP}}{\left(\theta_{OQR}\theta_{ORP}\right)^{\alpha}+\left(\theta_{ORP}\theta_{OPQ}\right)^{\alpha}+\left(\theta_{OPQ}\theta_{OQR}\right)^{\alpha}},\\ \left(u_z^w\right)_{A'}^{n+\frac{1}{2}}&=\frac{\left(\theta_{OQR}\theta_{ORP}\right)^{\alpha}\left(u_z\right)_{OPQ}+\left(\theta_{ORP}\theta_{OPQ}\right)^{\alpha}\left(u_z\right)_{OQR}+\left(\theta_{OPQ}\theta_{OQR}\right)^{\alpha}\left(u_z\right)_{ORP}}{\left(\theta_{OQR}\theta_{ORP}\right)^{\alpha}+\left(\theta_{ORP}\theta_{OPQ}\right)^{\alpha}+\left(\theta_{OPQ}\theta_{OQR}\right)^{\alpha}}\end{aligned} \tag{42}$$

where α is a parameter, usually with the value 1 or 2. Finally, the derivatives computed with the $a-\varepsilon-\alpha-\beta$ scheme are weighted averages between the values $(u_x^a)_{A'}^{n+\frac{1}{2}}$ and $(u_z^a)_{A'}^{n+\frac{1}{2}}$ calculated from the system, equation (29(a)-(c)), $(u_x^c)_{A'}^{n+\frac{1}{2}}$, $(u_z^c)_{A'}^{n+\frac{1}{2}}$ obtained with equation (38) and $(u_x^w)_{A'}^{n+\frac{1}{2}}$, $(u_z^w)_{A'}^{n+\frac{1}{2}}$ calculated with equation (42), i.e.

$$\begin{aligned}\left(u_x^{a-\varepsilon-\alpha-\beta}\right)_{A'}^{n+\frac{1}{2}}&=\left(u_x^a\right)_{A'}^{n+\frac{1}{2}}+2\varepsilon\left[\left(u_x^c\right)_{A'}^{n+\frac{1}{2}}-\left(u_x^a\right)_{A'}^{n+\frac{1}{2}}\right]\\ &\quad+\beta\left[\left(u_x^w\right)_{A'}^{n+\frac{1}{2}}-\left(u_x^c\right)_{A'}^{n+\frac{1}{2}}\right],\\ \left(u_z^{a-\varepsilon-\alpha-\beta}\right)_{A'}^{n+\frac{1}{2}}&=\left(u_z^a\right)_{A'}^{n+\frac{1}{2}}+2\varepsilon\left[\left(u_z^c\right)_{A'}^{n+\frac{1}{2}}-\left(u_z^a\right)_{A'}^{n+\frac{1}{2}}\right]\\ &\quad+\beta\left[\left(u_z^w\right)_{A'}^{n+\frac{1}{2}}-\left(u_z^c\right)_{A'}^{n+\frac{1}{2}}\right].\end{aligned} \tag{43}$$

The authors of the method (Chang *et al.*, 1998) indicate that the numerical dissipation introduced by the ε term is effective in damping out numerical instabilities that occur in the smooth regions of the solution, while the $\alpha-\beta$ term is effective in damping out the wiggles that can occur in the vicinity of the solution discontinuities. Stability requires, besides the CFL condition, that $a-\varepsilon-\alpha-\beta$ scheme must also satisfy the following conditions

$$0 \le \varepsilon \le 1, \quad \beta \ge 0, \quad \alpha \ge 0. \tag{44}$$

The $a - \varepsilon$ scheme can be considered as a particular case of the $a - \varepsilon - \alpha - \beta$ method for $\beta = 0$ or $\alpha = 0$, while the a scheme can be obtained when the supplementary condition $\varepsilon = 0$ is satisfied. The most computationally efficient scheme, as previously shown, is obtained for $\varepsilon = 0.5$ because in this case, the method is purely (global and local) explicit; only this case has been used to obtain the results shown in the next section of this work.

Considering that at one half-time step, the values u, u_x, u_z have been calculated for point A', the values of the same dependent variables can be determined at the same half-time step at any other point inside the hexagon *BECFDG* using the simplified Taylor expansion (equation (18)), (without the time dependent term) and considering that u_x and u_z are constant over the surface of the hexagon.

Figure 4 shows a simple, uniform, grid. On one half-time step, the values of the dependent variables u, u_x, u_z are calculated for one set of triangular elements (centers), like those marked with dark points in the figure. At the next half-time step the other set of triangular elements are considered – marked with hollow circles. At the next time step, the first set of elements are considered again; in conclusion, two half-time steps are necessary to return to one set of elements.

An alternative method of estimating u_x and u_z at the new time step has been proposed recently (Liu and Chen, 2001). This method requires, at each half-time step, the calculation of the new value variable u for all triangular elements. In a similar way with the $a - \varepsilon - \alpha - \beta$ method, consider in the three-dimensional space (x, z, u) four points defined as $O\left(x_{A'}, z_{A'}, u_{A'}^{n+\frac{1}{2}}\right)$, $P_1\left(x_{E'}, z_{E'}, u_{E'}^{n+\frac{1}{2}}\right)$, $Q_1\left(x_{F'}, z_{F'}, u_{F'}^{n+\frac{1}{2}}\right)$ and $R_1\left(x_{G'}, z_{G'}, u_{G'}^{n+\frac{1}{2}}\right)$. Three planes can be considered, each defined by a set of three points: OP_1Q_1, OQ_1R_1 and OR_1Q_1. Considering that

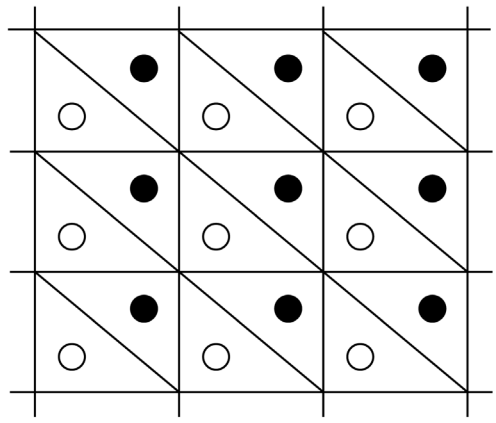

Figure 4.
Uniform triangular mesh

function u is linear both in x and in z directions over the domains defined by these planes, the partial derivatives can easily be calculated over the three domains (triangles OP_1Q_1, OQ_1R_1 and OR_1Q_1) using equations similar with equations (36) and (37). Let $(u_x)_{OP_1Q_1}$, $(u_z)_{OP_1Q_1}$, $(u_x)_{OQ_1R_1}$, $(u_z)_{OQ_1R_1}$ and $(u_x)_{OR_1P_1}$, $(u_z)_{OR_1P_1}$ be these values, respectively. The partial derivatives at the new time step can now be estimated using equations similar to equations (40)-(42). No ε-type artificial dissipation is introduced.

No significant differences between the results obtained using any of the above artificial dissipation schemes have been observed.

In conclusion, the unknowns at the new half-time step $n+\frac{1}{2}$ are calculated as functions of the old half-time step n using explicit expressions (equations (30) and (43)). At this stage, the grid is shifted. For example, when at time step n the variables are known at the dark nodes (Figure 4), at the half-time step $n+\frac{1}{2}$ the unknowns are calculated at the hollow nodes (Figure 4). It takes another half-time step, $n+\frac{1}{2}\rightarrow n+1$, for the grid to return to the dark nodes. This peculiarity explains the half-time division. Also, the fact that the derivatives are not calculated directly from the conservation laws (which was the price paid for making the scheme fully explicit) does not diminish the value of the method: the conservation laws are still satisfied within the larger, hexagonal elements. The method is simultaneously accurate (the conservation is satisfied both in space and time for the hexagonal elements) and explicit (computationally efficient). It is these characteristics that provide the strength of the CE/SE method.

Results and discussion

In order to determine the performance of the method, several numerical examples are considered. The results are compared with the results obtained from other numerical methods, as well as with experimental data. Only the steady state solution, obtained by time integration until the state parameters stabilize, is considered.

Circular journal bearing

A standard journal bearing with one inlet groove is first considered. The geometry and the fluid characteristics are presented in Table I.

Figures 5 and 6 show a comparison between the pressure distributions and the fluid film content θ obtained with CE/SE method and with the type difference method (Vijayaraghavan and Keith, 1989). Two transverse sections through the bearing at $z=0$ and $z=L/4$ are presented for each method. Note that the bearing z coordinate ranges between the values $-L/2\leq z\leq L/2$ so that $z=0$ is the symmetry plane. The differences between the two methods are relatively small; the maximum pressure predicted using type differencing is 6.7 percent lower than the maximum pressure calculated with the present method, while the total load is only 1.3 percent lower. The difference between

the attitude angles calculated with the two methods is 0.4°. Two cavitated regions, $\theta < 1$, are visible. The larger one is located immediately before the lubricant supply position, and it will be discussed in the following paragraph. The smaller cavitated region is located around 162° circumferential coordinate. Figure 6 shows that for this second cavitated region, both methods predict $\theta \approx 1$ at the symmetry plane, $z = 0$, and $\theta < 1$ at $z = L/4$ which indicates that the cavitation is more pronounced toward the ends of the bearing than at the center.

Parameter	Value	Units
Length	26.0×10^{-3}	m
Diameter	45.0×10^{-3}	m
Clearance	15.0×10^{-6}	m
Relative eccentricity	0.8	–
Lub. supply position	120	deg
Supply pressure (gage)	5.458×10^{5}	Pa
Velocity	3952	rot/min
Viscosity	0.00325	Pa s
Bulk modulus (β')	1.21×10^{8}	Pa
Cavitation pressure (gage)	0	N/m^2

Table I.
Physical conditions for circular journal bearing

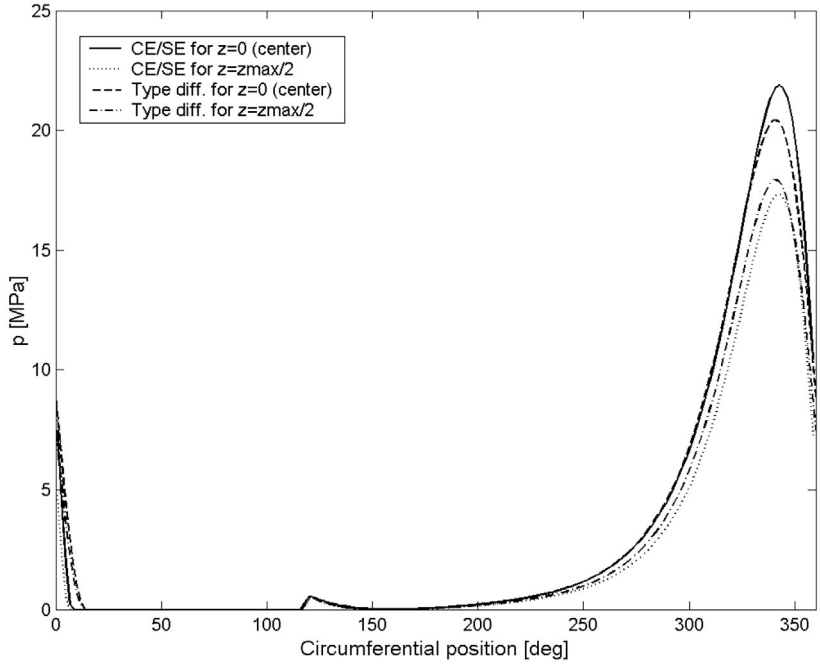

Figure 5.
Pressure distribution for a circular journal bearing with one inlet groove

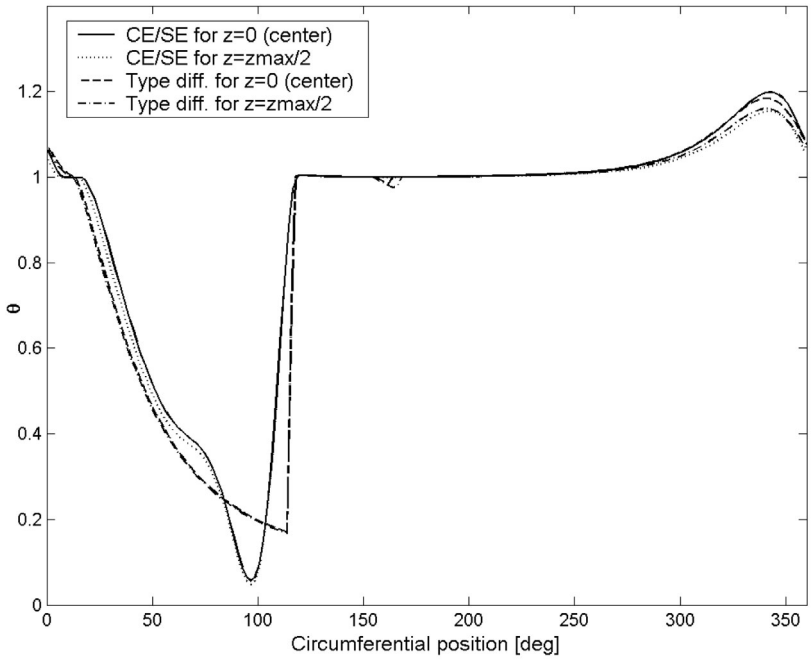

Figure 6.
Fractional film content distribution for a circular journal bearing with one inlet groove

In Figure 6, for the larger cavitated region, the type differencing method seems to be able to handle the large discontinuity for the fractional film content better than the CE/SE method. However, the discontinuity was not actually calculated in the type differencing code results. Rather, two boundaries (the two sides of the lubricant supply pocket) are next to the other, so that the sharp discontinuity in the fractional film content distribution is only due to the geometry. On the other hand, the computational domain used by CE/SE code is continuous (periodic boundary conditions are used at one circumferential position), so that the fractional film content discontinuity naturally appears in the field. This approach was possible only because this method is able to cope with large discontinuities without introducing significant numerical smearing and/or oscillations. The code developed using this method is thus more general and can be applied to bearings where the computational domain cannot be split at the lubricant location (when the supply pocket is inside the bearing, without reaching the bearing margins).

Wave journal bearing

The geometry of a wave bearing is more complex compared to the geometry of a standard journal bearing (Dimofte, 1995). An example of the film thickness

distribution for a three wave bearing as a function of the circumferential coordinate is shown in Figure 7. The other physical conditions are presented in Table II.

Figure 8 shows the pressure distribution obtained using the present method compared with the pressure calculated by Dimofte (1995), using a finite difference method to solve the steady form of Reynolds equation with

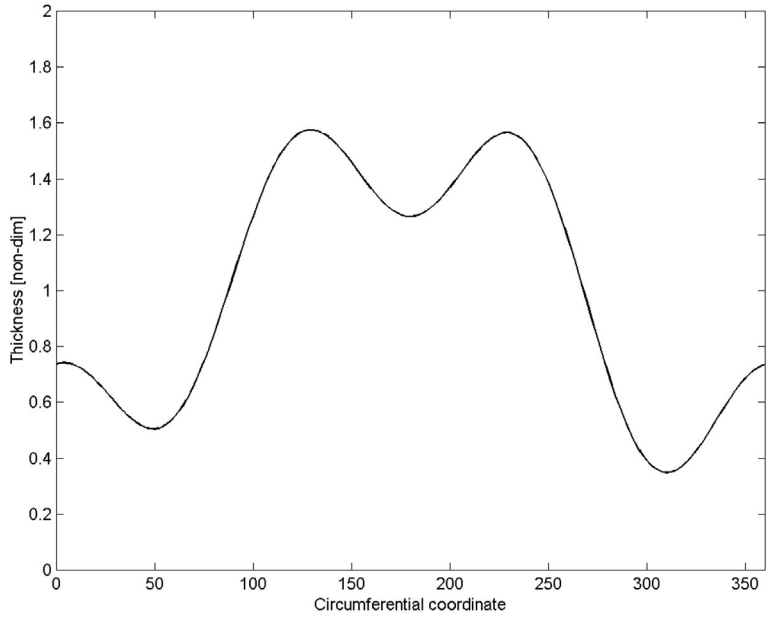

Figure 7.
Fluid film thickness distribution in a three-wave bearing

Parameter	Value	Units
Length	26.0×10^{-3}	m
Diameter	45.0×10^{-3}	m
Clearance	15.0×10^{-6}	m
Number of supply pockets	3	–
Lub. supply positions	86, 206, 326	deg
Supply pockets width	4.0	mm
Supply pressure (gage)	5.458×10^{5}	Pa
Velocity	3952	rot/min
Viscosity	0.00325	Pa s
Density	902.0	Kg/m^3
Bulk modulus $\beta'(\bar{\beta}')$	1.2105×10^{8} (40.0)	Pa
	1.029×10^{7} (3.4)	
Cavitation pressure (gage)	0	N/m^2

Table II.
Physical conditions for wave bearing

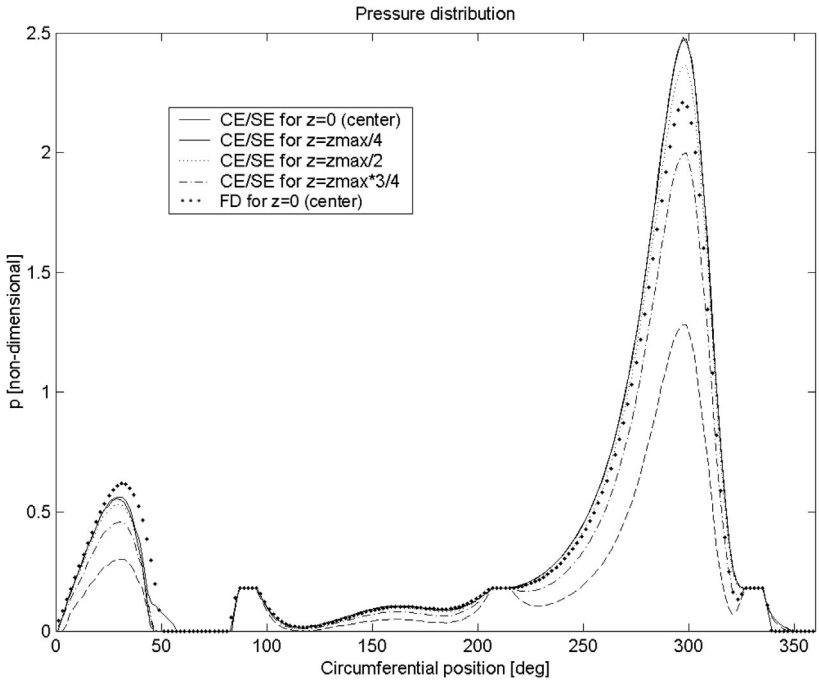

Figure 8.
Pressure distribution in a wave bearing $\bar{\beta}' = 40.0$

Gümbel (or half-Sommerfeld) boundary conditions. The results show similar variations, however the peak pressures differ. The total load predicted by the present method is 2,039 N, 13.7 percent higher than the load predicted by Dimofte (1995). The difference between the predicted load directions using the two codes is less than 1.6°. These results have been obtained using a value $\beta' = 1.2105 \times 10^8$ Pa. For a lower value $\beta' = 1.029 \times 10^7$ Pa, the pressure distribution is shown in Figure 9. In this case, even though both peak pressures predicted by the present method and Dimofte are almost the same, the total load compared with the previous case does not change significantly. The load directions however, have a larger difference (5.5°). In brief, the film compressibility effects reduce the pressure peaks in the bearing and also produce a change in the pressure distribution phase. Note that, although the bulk modulus value for the oil used by Dimofte is not known, the first case ($\beta' = 1.2105 \times 10^8$ Pa) probably uses a more realistic value. Note as well that the code based on the present method uses a film thickness distribution calculated by Dimofte considering the elastic deformations of the shaft and bushing; this can also be a source of error.

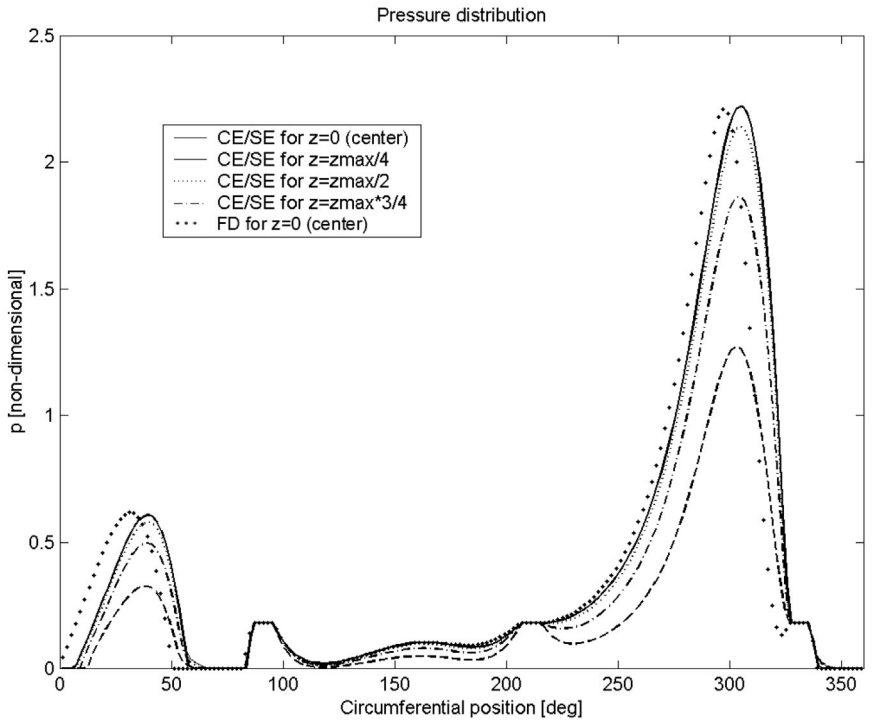

Figure 9.
Pressure distribution in a wave bearing $\bar{\beta}' = 3.4$

Misaligned wave journal bearing

The misalignment of journal bearings can be defined using two parameters: the angle α between the centerline and the direction of the misalignment at the bearing center and the degree of misalignment d_m that represents the proportion of the actual misalignment from the maximum possible. The misalignment is restricted by the condition that at the bearing axial ends the film thickness reaches the value of zero. The physical conditions of the bearing are presented in Table III. Because of the misalignment, the fluid film thickness is a function of both the circumferential and axial coordinates, so that for each value of the circumferential coordinate there exists a domain of thickness variation, represented in dark color in Figure 10.

The pressure distribution in the bearing is shown in Figures 11(a) and 12(a), while the fractional fluid film content is shown in Figure 13(a). The same bearing with the same physical conditions and without misalignment shows different values for the pressure distribution and fractional film content, as seen in Figures 11(b), 12(b) and 13(b). The cavitation, respectively, the full film regions for the misaligned and the aligned three-wave bearing are shown in Figure 14(a) and (b). The load is 20,988 N for the aligned bearing and 36,100 N

Parameter	Value	Units
Length	45.0×10^{-3}	m
Diameter	45.0×10^{-3}	m
Clearance	15.0×10^{-6}	m
Angle of misalignment	90	deg
Degree of misalignment	0.5	–
Number of supply pockets	1	-
Lub. supply position	100	deg
Supply pocket width	4.0	mm
Supply pressure (gage)	5.458×10^{5}	Pa
Velocity	3952	rot/min
Viscosity	0.00325	Pa s
Density	902.0	Kg/m^3
Bulk modulus $\beta'(\bar{\beta}')$	1.2105×10^{8} (40.0)	Pa
Cavitation pressure (gage)	0	N/m^2

Table III.
Physical conditions for misaligned wave bearing

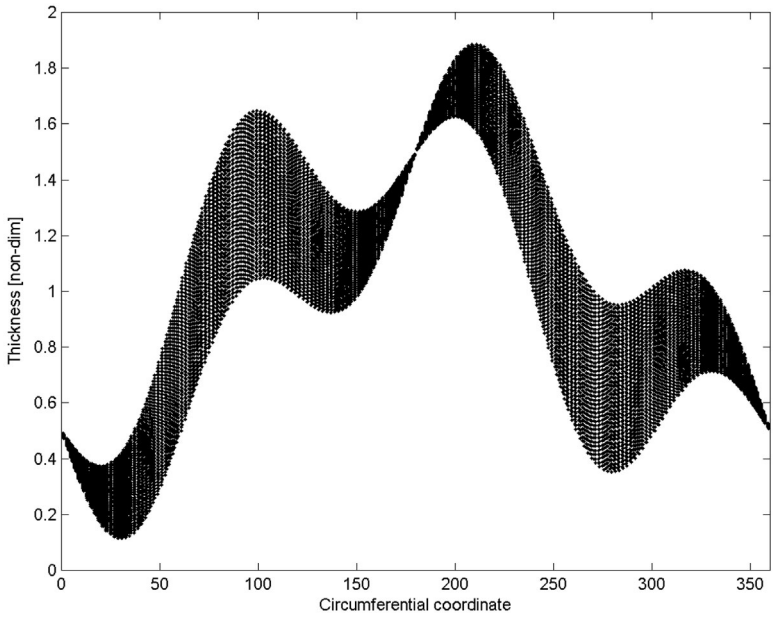

Figure 10.
Fluid film thickness domain in a misaligned three-wave bearing

for the misaligned bearing, which shows that sometimes misalignment can have a positive impact on bearing performance. This effect is due to the expanded full film region that permits the development of higher pressures inside the misaligned bearing.

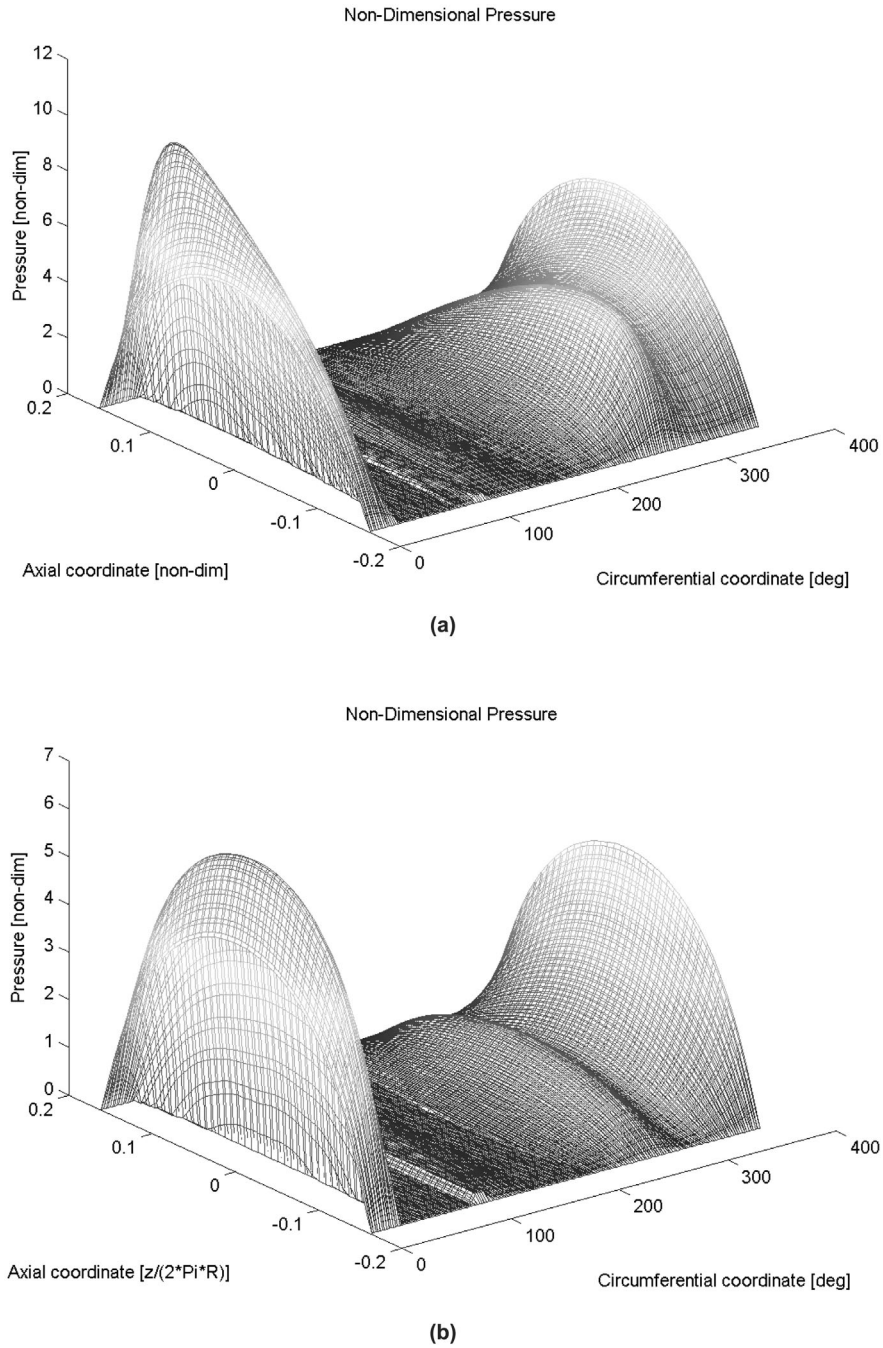

Figure 11.
(a) Pressure distribution in a misaligned three-wave bearing. (b) Pressure distribution in a three-wave bearing

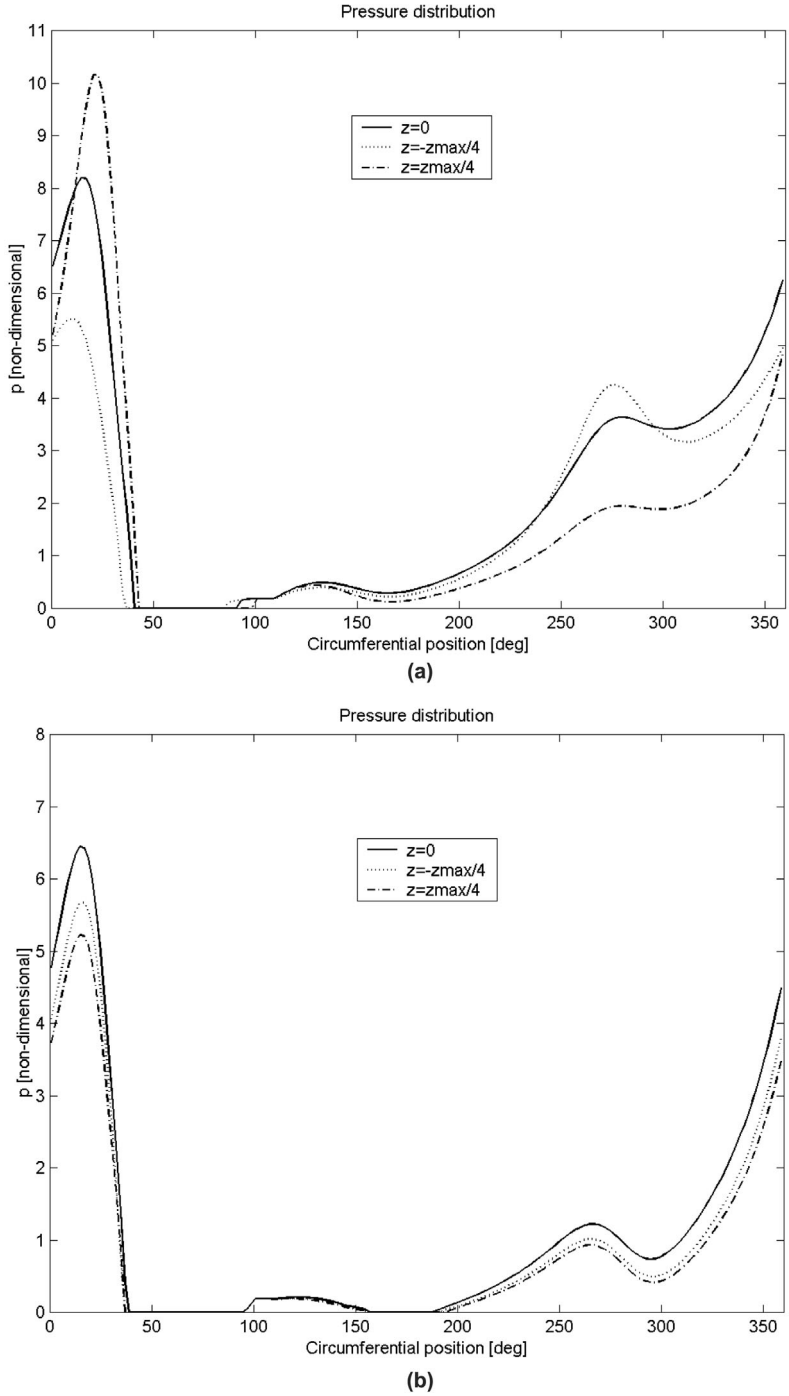

Figure 12.
(a) Pressure distribution in a misaligned three-wave bearing at different axial sections.
(b) Pressure distribution in an aligned three-wave bearing at different axial sections

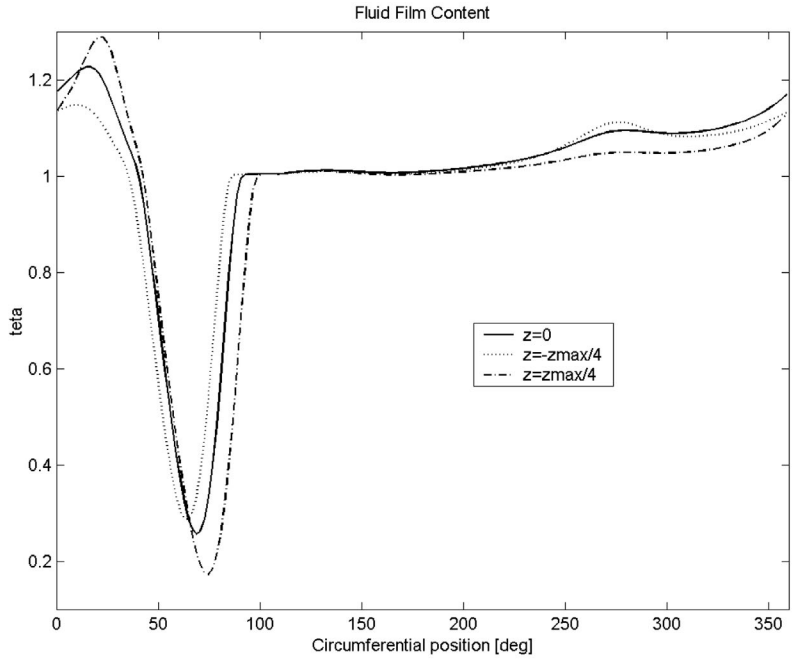

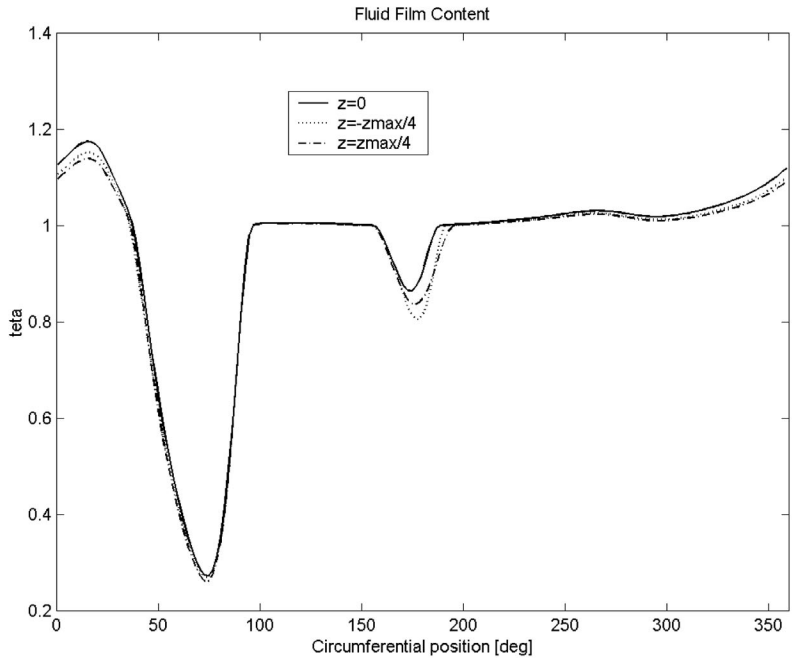

Figure 13.
(a) Fractional film content distribution in a misaligned three-wave bearing at different axial sections (b) fractional film content distribution in an aligned three-wave bearing at different axial sections

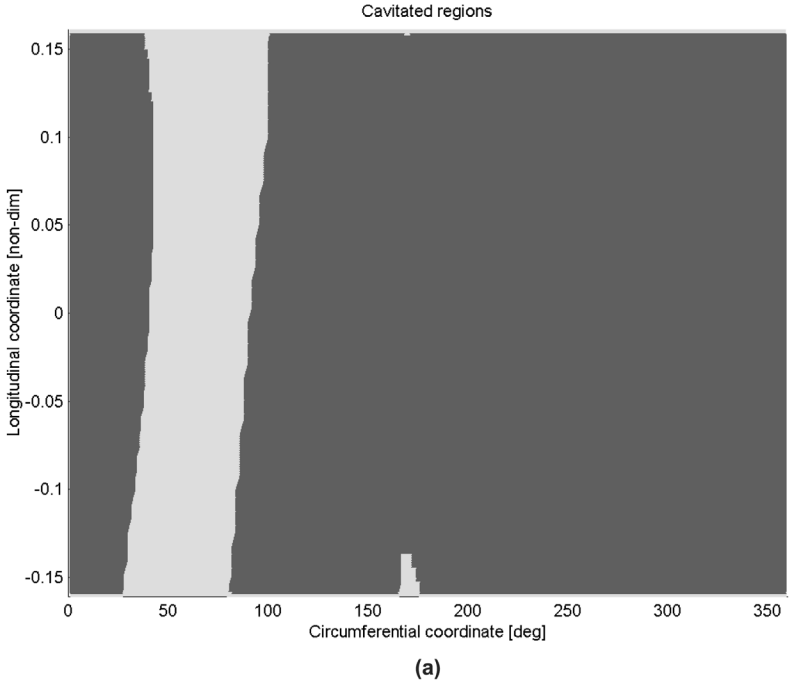

Figure 14.
(a) Cavitation map in a misaligned three-wave bearing. (b) Cavitation map in an aligned three-wave bearing

Conclusions

The CE/SE method was applied for the first time to investigate two-dimensional flow in cavitated bearings. Contrasted with other numerical schemes, the space-time CE/SE method insures conservation both in space and time, so it is potentially more accurate. The theoretical formulation of the problem was presented along with the numerical results obtained for different types of bearings. The results were compared with the results obtained using other numerical algorithms. The comparison shows that the CE/SE method, when contrasted to previous numerical algorithms, can successfully predict pressure distribution within bearings, including cases with discontinuities in the lubricant film, without any special treatment. It is also important to recognize that the CE/SE method is conceptually simple and entirely explicit, which makes it also computationally efficient.

References

Chang, S.C. and To, W.M. (1991), "A new numerical framework for solving conservation laws – the method of space-time conservation element and solution element", *NASA TM 104495*, NASA, Cleveland, OH.

Chang, S.C., Wang, X.Y. and Chow, C.Y. (1999), "The space-time conservation element and solution element method: a new high-resolution and genuinely multidimensional paradigm for solving conservation laws", *J. Comp. Phys.*, Vol. 156 No. 1, pp. 89-136.

Chang, S.C. *et al.* (1998), "Fundamentals of CE/SE method", *NASA TM-1998-208843*, PDF file http://www.grc.nasa.gov/WWW/microbus/cese/ltxjcp2d.pdf, Cleveland, OH.

Cioc, S. and Keith, T.G. Jr (2002), "Application of the CE/SE method to one-dimensional flow in fluid film bearings", *STLE Tribology Transactions*, Vol. 45 No. 2, pp. 169-76.

Dimofte, F. (1995), "Wave journal bearing with compressible lubricant – part I: the wave bearing concept and a comparison to the plain circular bearing", *STLE Tribology Transactions*, Vol. 38 No. 1, pp. 153-60.

Elrod, H.G. (1981), "A cavitation algorithm", *ASME J. Lubr. Tech.*, Vol. 103 No. 3, pp. 350-4.

Jakobsson, B. and Floberg, L. (1957), "The finite journal bearing considering vaporization", *Transactions of Chalmers University of Technology*, Gothenburg, Sweden, p. 190.

Liu, N.S. and Chen, K.H. (2001), "An alternative flow solver for the NCC — the FLUX code and its algorithm", *AIAA Paper 2001-0973*.

Olsson, K.O. (1965), "Cavitation in dynamically loaded bearings", *Transactions of Chalmers University of Technology*, Gothenburg, Sweden, p. 308.

Qin, J.R., Yu, S.T.J., Zhang, Z.C. and Lai, M.C. (2001), "Direct calculations of cavitating flows by the space-time CE/SE method", *Eleventh International Multidimensional Engine Modeling User's Group Meeting*, Detroit, MI, http://www.erc.wisc.edu/multi_dimensional/ModelingMtng2001/Yu_Lai.pdf

Vijayaraghavan, D. and Keith, T.G. Jr (1989), "Development of a cavitation algorithm", *Trib. Trans.*, Vol. 32 No. 2, pp. 225-33.

Vijayaraghavan, D., Keith, T.G. Jr and Brewe, D.E. (1990), "Extension of transonic flow computational concepts in the analysis of cavitated bearings", *NASA TM-103214*, NASA, Cleveland, OH.

Wang, X.Y., Chang, S.C. and Jorgenson, P.C.E. (2000), "Prediction of sound waves propagating through a nozzle without/with a shock wave using the space-time CE/SE method", *NASA TM – 2000-209937*.

Further reading

Chang, S.C., Loh, C.Y., Yu, S.T., Himansu, A., Wang, X.Y. and Jorgenson, P.C.E. (1997), "Robust and simple non-reflecting boundary conditions for the space-time conservation element and solution element method", *AIAA*, *Paper 97-2077*.

Vijayaraghavan, D. (1989), "New concepts in numerical prediction of cavitation in bearings", *PhD dissertation*, The University of Toledo.